Hindawi
Advances in Civil Engineering
Volume 2023, Article ID 9278321, 16 pages
https://doi.org/10.1155/2023/9278321

Research Article

A Novel Method for Deflection Calculation of Reinforced Concrete Stair Slabs considering Step Stiffness

Xiuzhong Peng and Chenhao Lu

School of Civil Engineering, Southeast University, Nanjing 211189, China

Correspondence should be addressed to Chenhao Lu; chenhao_lu@seu.edu.cn

Received 29 August 2022; Revised 29 March 2023; Accepted 5 April 2023; Published 22 April 2023

Academic Editor: Iman Mansouri

Stair slabs are some of the most common structural members with zigzag shapes in various buildings. However, the calculated deflection is usually overestimated during the design of stair slabs. In this article, the overestimated deflection is amended by utilizing step stiffness. To this end, it is assumed that the stress distribution of a unit cell in stair slabs is linear or bilinear under a constant bending moment. Stair slabs can be approximately regarded as flat slabs to derive the equivalent thickness based on the same bending strain energy. Subsequently, finite element (FE) models are established to verify that the obtained equivalent thickness can be applied to reinforced concrete (RC) stair slabs. To improve computational efficiency, the normalized models of stair slabs are adopted for further analysis. On this basis, a novel design method is proposed considering step stiffness for RC stair slabs. Furthermore, numerical examples are presented to compare the improved design method with the FE method and the conventional method. The results demonstrate that the design method considering step stiffness can not only ensure structural safety but also reduce concrete and steel consumption, making the design of stair slabs more economical and reasonable.

1. Introduction

Reinforced concrete (RC) stair slabs are supported on two opposite sides to connect planes at different heights, having the advantages of simple appearances, clear load transmission paths, and convenient construction. The shape of stair slabs is generally zigzag. In the previous studies [1–3], the analysis and design of stair slabs were conducted using the minimum cross-sectional depth perpendicular to the bottom surface. In some cases, it is found that the designed stair slabs are quite thick to control deflection, leading to a headroom problem. However, the experiments [4] pointed out that steps play a part in resisting the external loads, significantly contributing to the overall stiffness of stair slabs. Therefore, it is necessary to properly consider the positive influence of step stiffness on deflection control during design.

Accurate estimation of the stiffness of stair slabs is a crucial issue. As flexural members, stair slabs can be considered as beams with periodically variable cross sections. In the past several decades, diverse methods have been proposed to solve the problems relating to the stiffness of variable cross-section beams, such as deflection prediction and vibration analysis. Some studies [5–7] concentrated on deriving the exact element stiffness matrix of beam elements with linearly variable cross-section dimensions based on the Euler–Bernoulli and Timoshenko beam theories. After that, displacement interpolation functions were improved to apply the beam elements to more member types with variable cross sections [8, 9]. Romano [10] established the fourth-order differential equations to get the analysis solutions of deflection for varying cross-section beams. Yoon and Lee [11] added three warping degrees of freedom to each node of beam elements to consider the shear deflection of varying cross-section beams. Huang et al. [12] divided the actual deflection into the homogenized deflection and the warping deflection to predict the effective stiffness of periodic beams. For vibration analysis of step beams with the abrupt change of cross sections, the conventional methods are the finite element (FE) method, the Rayleigh method,

and the component modal analysis [13, 14]. Moreover, a few innovative approaches were developed to improve the accuracy and efficiency of vibration analysis, such as Green's function method [15], the composite element model [16], the Adomain decomposition method [17], the differential quadrature element method [18], the discrete singular convolution algorithm [19], and the elemental impedance method [20].

Despite these advances, the predicted stiffness and natural frequency of variable cross-section beams are larger than the experimental results in most cases. El-Mezaini et al. [21] attributed it to neglecting the stiffness reduction caused by the small stress regions existing in the variable cross-section members. On the basis of the explanation, Zheng and Ji [22, 23] created a unified expression of equivalent inertia moment for periodic beams to estimate deflection and natural frequency. In addition, Xu et al. [24] removed the small stress regions on steps to secure an analytic solution of equivalent thickness for RC stair slabs. Though it is convenient and efficient to predict the stiffness of variable cross-section members via the calculation formulas [22–24], the stress distribution in members is oversimplified in the derivation process. As a result, the application of such methods is limited to the range of members with simple shapes. In terms of periodic beams with a complicated microstructure, further studies [25–27] combined the asymptotic homogenization method and the finite element method to compute the effective stiffness of the beams. However, for the asymptotic homogenization method, the finite element analysis requires to be implemented iteratively in different boundary conditions, increasing computational cost. Consequently, more accurate and efficient approaches should be developed to obtain the overall stiffness of periodically variable cross-section members.

This article aims to propose a novel method to calculate the deflection of stair slabs with consideration of step stiffness. In the elastic range, the stress distribution in a unit cell is assumed to derive the equivalent thickness of stair slabs. Then, the nonlinear FE analysis is conducted to ensure the applicability of the obtained equivalent thickness in RC stair slabs. Based on the Chinese codes [28, 29], an improved design method for RC stair slabs is suggested. Subsequently, numerical examples are implemented to illustrate the reliability and advantages of the proposed design method in comparison with the FE method and the conventional method.

2. Theoretical Analysis for Equivalent Thickness of Stair Slabs

A stair slab consists of an inclined slab and a series of identical steps, as shown in Figure 1(a). The relationship among geometric parameters of the stair slab is expressed as follows:

$$k = \tan\theta = \frac{h}{b}, \tag{1}$$

where k is the slope of the stair slab, θ is the inclined angle of the stair slab, h is the height of each step, and b is the width of each step.

For simplicity of analysis, a unit cell is taken from the stair slab with the width w, as depicted in Figure 1(a). The unit cell can be split into two parts. One part is subjected to very small stresses and expressed as "the part ABC," and the other part, of which upper boundaries are called "the path A-C-D," could effectively provide stiffness for the stair slab. The assumed normal stresses in the path A-C-D for the unit cell are illustrated in Figure 1(b). A Gaussian coordinate system of the unit cell is established in Figure 1(c). The corresponding equivalent flat slab is shown in Figure 1(d). The length of each unit cell along the x direction s is written as follows:

$$s = \sqrt{b^2 + h^2}. \tag{2}$$

2.1. Basic Assumptions. In the unit cell analysis model as illustrated in Figure 1(c), the geometry of the unit cell is the combination of a triangular step and a rectangular slab. The basic geometric parameters, which determine the dimensions of the unit cell, contain the height of the step h, the width of the step b, the thickness of the slab t, and the width of the slab w. Note that the material of the unit cell considers only concrete, but steel rebars are excluded. This is because the main factors to influence the overall stiffness of stair slabs within the elastic range are the geometry, dimensions, and properties of concrete, rather than the quantity, positions, and properties of steel rebars. Furthermore, the boundary conditions of the analysis model are a pin support at one end and a roller support at the other, making the unit cell remain pure bending when a bending moment is applied.

To simplify the derivation process of equivalent thickness within the elastic range, the assumptions relating to the unit cell in Figure 1(c) are as follows:

(1) To make stairs as comfortable to walk up and down as possible, the height h and the width b in a step should satisfy the following equation [30]:

$$T = 2h + b, \tag{3}$$

where T is the characteristic length of steps, which varies from 550 to 700 mm and should be close to 630 mm [30].

(2) The material of the unit cell is homogeneous, isotropic, and linearly elastic. Its elastic modulus is represented by E.

(3) A constant bending moment M is applied in the unit cell so that the upper part of the unit cell is in compression and the lower part is in tension, as shown in Figure 1(c).

(4) The part ABC in Figure 1(c) is denoted as "the ineffective region" due to the extremely small contribution to the stiffness of stair slabs, and the other part is termed "the effective region" [22]. Two lines AC and CD are the upper boundaries of the effective region in Figure 1(c). The angle of the line AC with respect to the x direction is assumed to be 30°. The projection lengths of the lines AC and CD on the x

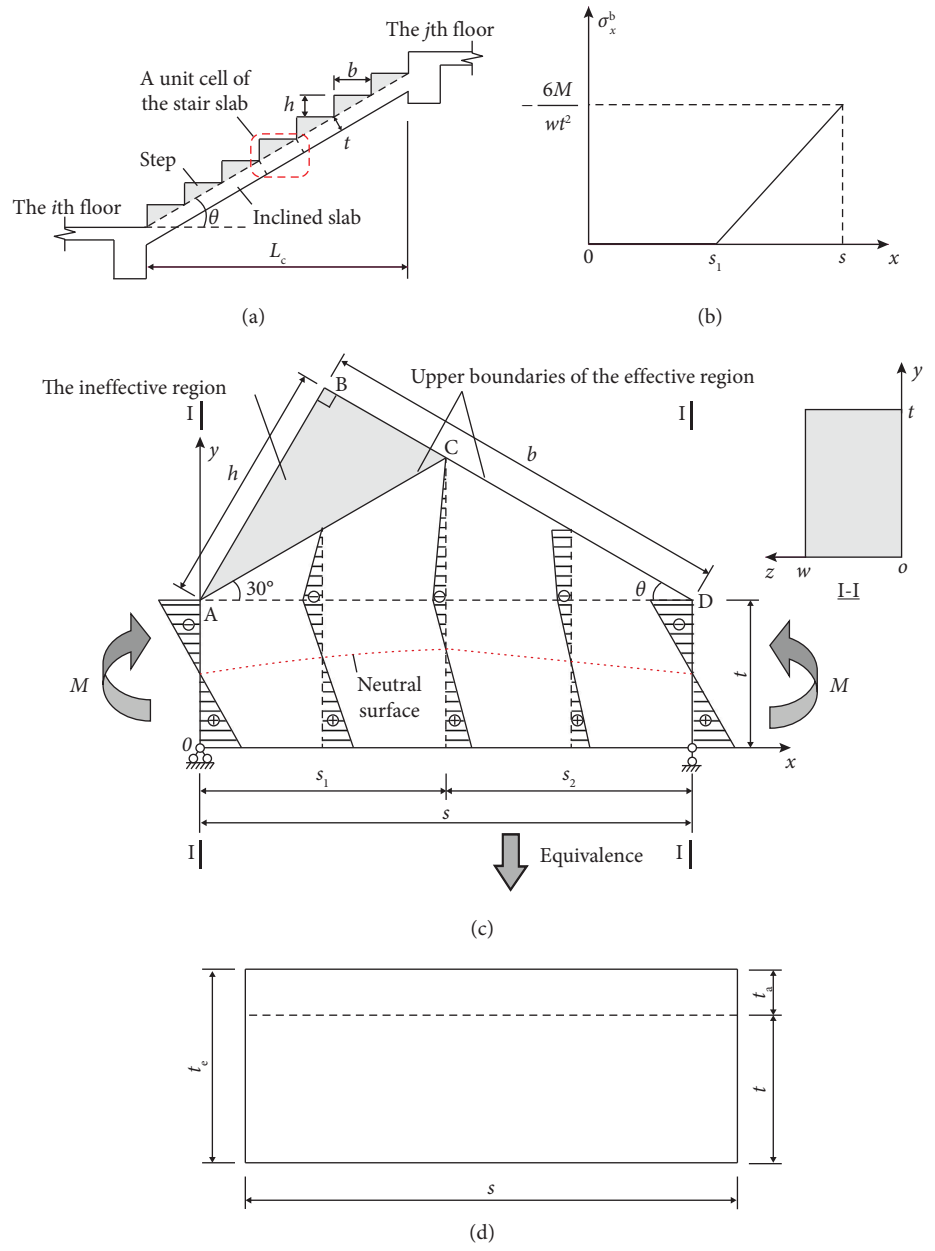

FIGURE 1: Schematicdiagrams of a stair slab and the analysis model of a unit cell. (a) A stair slab consisting of an inclined slab and a series of identical steps. (b) The assumed normal stresses in the path A-C-D for the unit cell. (c) The normal stress distribution of the unit cell. (d) The equivalent flat slab.

axial are s_1 and s_2, respectively. The lengths s_1 and s_2 are obtained as follows:

$$s_1 = \frac{\sqrt{3}ks}{\sqrt{3}k+1}, \qquad s_2 = \frac{s}{\sqrt{3}k+1}. \tag{4}$$

(5) The normal stress distribution in the unit cell is linear or bilinear as shown in Figure 1(c), and the slope of the normal stress changes at $y = t$. The normal stress function $\sigma_x^b(x)$ in the path A-C-D in Figure 1(b) is given as follows:

$$\sigma_x^b(x) = \begin{cases} -\dfrac{6M}{wt^2}, & x = 0, \\ 0, & 0 < x \le s_1, \\ -\dfrac{6M}{s_2 wt^2}(x - s_1), & s_1 < x \le s. \end{cases} \tag{5}$$

(6) The location of the neutral axis and the radius of curvature in the unit cell vary linearly in the range of $x = s_1$ to $x = s$.

(7) The bending strain energy in the unit cell is the same as that in the corresponding equivalent flat slab.

2.2. Derivation of Equivalent Thickness. For simplicity, the ineffective region is omitted in the analysis process. Within the elastic range, the derivation of equivalent thickness is given in the following:

In Figure 1(c), the vertical distance function $u(x)$ from the x axis to the lines AC and CD is written as follows:

$$u(x) = \begin{cases} \dfrac{x}{\sqrt{3}} + t, & 0 \le x \le s_1, \\ -k(x - s) + t, & s_1 < x \le s. \end{cases} \tag{6}$$

Using equations (1) and (3), the height h and the width w in a step can be derived as follows:

$$h = \frac{Tk}{2k+1}, \qquad b = \frac{T}{2k+1}. \tag{7}$$

In the range from $x = 0$ to $x = s_1$, the stress distribution on the cross section at $x = x_0$ is plotted in Figure 2. For ease of analysis, the distance function $g(x)$ from the x axis to the neutral axis and the curvature function $\varphi(x)$ are introduced.

In Figure 2, the resultant force F_t on the tension zone at $x = x_0$ is calculated as follows:

$$\begin{aligned} F_t &= \int_0^{g(x_0)} E w \varphi(x_0)(g(x_0) - y)\mathrm{d}y, \\ &= \frac{1}{2} E w \varphi(x_0) g^2(x_0). \end{aligned} \tag{8}$$

It is noticed that the resultant force on the compression zone at $x = x_0$ is composed of the resultant force F_{c1} in the range from $y = g(x_0)$ to $y = t$ and the resultant force F_{c2} in the range from $y = t$ to $y = u(x_0)$. The resultant forces F_{c1} and F_{c2} are computed as follows:

$$\begin{aligned} F_{c1} &= \int_{g(x_0)}^{t} E w \varphi(x_0)(y - g(x_0))\mathrm{d}y \\ &= \frac{1}{2} E w \varphi(x_0)(t - g(x_0))^2, \end{aligned} \tag{9}$$

$$\begin{aligned} F_{c2} &= \int_t^{u(x_0)} \frac{E w \varphi(x_0)(t - g(x_0))}{u(x_0) - t}(u(x_0) - y)\mathrm{d}y \\ &= \frac{1}{2} E w \varphi(x_0)(t - g(x_0))(u(x_0) - t). \end{aligned} \tag{10}$$

Based on the equilibrium condition that the resultant force on the tension zone is equal to that on the compression zone, the relationship among the resultant forces F_t, F_{c1}, and F_{c2} is given by the following equation:

$$F_t = F_{c1} + F_{c2}. \tag{11}$$

Consequently, equations (8)–(11) together result in the location of the neutral axis at $x = x_0$, which is expressed as follows:

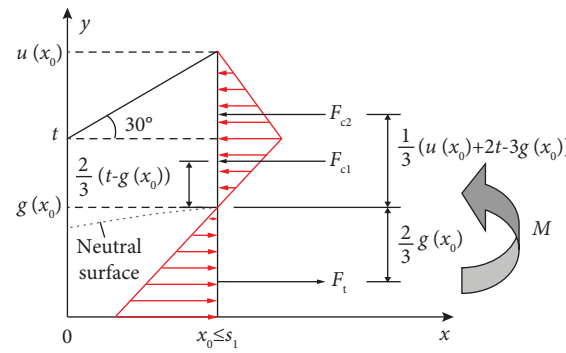

FIGURE 2: The stress distribution on the cross section at $x = x_0$ in the range from $x = 0$ to $x = s_1$.

$$g(x_0) = \frac{t u(x_0)}{t + u(x_0)}. \tag{12}$$

In addition, considering that the normal stress distribution is linear at $x = s$, the distance of the neutral axis to the x axis at $x = s$ is $t/2$. Then, according to equation (12) and the sixth assumption (the location of the neutral axis varies linearly in the range of $x = s_1$ to $x = s$), the location function $g(x)$ of the neutral axis in the range of $x = 0$ to $x = s$ is summarized as follows:

$$g(x) = \begin{cases} \dfrac{t u(x)}{t + u(x)}, & 0 \le x \le s_1, \\ -\dfrac{\sqrt{3}\, kt(x - s)}{2(2\sqrt{3}\, t + s_1)} + \dfrac{t}{2}, & s_1 < x \le s. \end{cases} \tag{13}$$

It is important to note that, in the range of $x = s_1$ to $x = s$, the resultant forces in the x direction acting on the cross sections might not be zero when using equation (13).

On the other hand, in Figure 2, equilibrium requires that the bending moment M and the sum of the moments provided by the resultant forces F_t, F_{c1}, and F_{c2} about the neutral axis are identical numerically, namely,

$$\begin{aligned} M = {} & \frac{2}{3} g(x_0) F_t + \frac{2}{3}(t - g(x_0)) F_{c1} \\ & + \frac{1}{3}(u(x_0) + 2t - 3g(x_0)) F_{c2}. \end{aligned} \tag{14}$$

By substituting equations (8)–(10) into equation (14), the curvature at $x = x_0$ can be obtained as follows:

$$\varphi(x_0) = \frac{12M}{\eta(x_0) E w t^3}, \tag{15}$$

where $\eta(x_0)$ is the value of the influence coefficient function $\eta(x)$ of step stiffness on the curvature when $x = x_0$. The influence coefficient function $\eta(x)$ is defined as follows:

$$\begin{aligned} \eta(x) = {} & \frac{2}{t^3}\big[(t + u(x))\big(t u(x) + 3g^2(x)\big) \\ & - left\big(t^2 + 4t u(x) + u^2(x)\big) g(x)\big], \ 0 \le x \le s_1. \end{aligned} \tag{16}$$

Moreover, the linear variation of normal stress at $x = s$ determines the curvature at $x = s$, which is equal to $12M/Ewt^3$. Afterwards, combining equation (15) and the sixth assumption (the radius of curvature varies linearly in the range of $x = s_1$ to $x = s$), the curvature function $\varphi(x)$ in the range of $x = 0$ to $x = s$ is given as follows:

$$\varphi(x) = \begin{cases} \dfrac{12M}{\eta(x)Ewt^3}, & 0 \le x \le s_1, \\ \dfrac{\varphi(s_1)\varphi(s)s_2}{(\varphi(s_1) - \varphi(s))(x - s_1) + \varphi(s)s_2}, & s_1 < x < s, \\ \dfrac{12M}{Ewt^3}, & x = s. \end{cases} \tag{17}$$

It should be noted that, in the range of $x = s_1$ to $x = s$, the external moment M could probably not be equal to the moment produced by the stress distribution about the neutral axis when using equation (17).

Subsequently, the distance function $d(x, y)$ from the neutral axis is introduced as follows:

$$d(x, y) = g(x) - y, \quad 0 \le y \le u(x). \tag{18}$$

The function $d(x, y)$ is positive when a given point is below the neutral axis and negative when above it.

Hence, the normal stress function $\sigma_x(x, y)$ in the unit cell is formulated as follows:

$$\sigma_x(x, y) = \begin{cases} E\varphi(x)d(x, y), & 0 \le x \le s, 0 \le y \le t \\ \dfrac{\sigma_x^{\mathrm{b}}(x) - E\varphi(x)d(x, t)}{u(x) - t}(y - u(x)) + \sigma_x^{\mathrm{b}}(x), & 0 \le x \le s, t < y \le u(x). \end{cases} \tag{19}$$

As a consequence, the bending strain energy V_e in the unit cell is derived as follows:

$$V_{\mathrm{e}} = \int_0^s \left(\int_0^{u(x)} \frac{\sigma_x^2(x, y)w}{2E} \mathrm{d}y \right) \mathrm{d}x. \tag{20}$$

By the seventh assumption (the bending strain energy remains the same after the stair slab is equivalent to the flat slab), the V_e can be rewritten as follows:

$$V_{\mathrm{e}} = \frac{6M^2 s}{Ewt_e^3}, \tag{21}$$

where t_e is the equivalent thickness of stair slabs.

From equation (21), the equivalent thickness t_e is solved as follows:

$$t_e = \sqrt[3]{\frac{6M^2 s}{EV_e w}}. \tag{22}$$

Note that the equivalent thickness t_e depends only on the characteristic length T, the inclined angle θ, and the thickness t, namely,

$$t_e = t_e(T, \theta, t). \tag{23}$$

To evaluate the contribution of steps to the stiffness of stair slabs, the additional thickness of stair slabs t_a is introduced as illustrated in Figure 1(d) and written as follows:

$$t_a = t_e - t. \tag{24}$$

The additional thickness t_a can be calculated from equations (1)–(24). The computation has been implemented in MATLAB in this study.

2.3. Solutions and Discussion. Table 1 lists the summary of t_a with different θ and t when T is 630 mm. The curved surface diagram of t_a varying with θ and t when T is 630 mm is visualized in Figure 3(a). The curves of t_a varying with t when $\theta = 20$ and 40° and $T = 550$, 630, and 700 mm are shown in Figure 3(b).

As can be seen from Figure 3(a), the additional thickness t_a increases with the growth of the inclined angle θ and the thickness t. The growth rate of the additional thickness t_a is approximately constant with respect to the inclined angle θ, whereas it decreases with the increase in the thickness t. It can be concluded that the larger the inclined angle θ and the thickness t are, the more contribution the steps make to the stiffness of stair slabs.

In Figure 3(b), when the inclined angle θ and the thickness t are determined, the difference of the additional thickness t_a between $T = 630$ mm and $T = 550$ mm is close to that between $T = 700$ mm and $T = 630$ mm. The result indicates that the additional thickness t_a is approximate to increase linearly as the characteristic length T increases and the contribution the steps make to the stiffness of stair slabs is positively related to the characteristic length T. Furthermore, it is recommended that when the inclined angle θ varies from 20 to 40° and the thickness t varies from 60 to 260 mm, Table 1 is applied to the design of stair slabs, neglecting the effect of the characteristic length T on the additional thickness t_a. This is because the maximum difference between the additional thickness t_a in Table 1 and its actual value is not larger than 3 mm in this situation, which is acceptable in engineering practice.

3. Finite Element Analysis and Validation

In this section, two RC stair slabs with different thicknesses (i.e., $t = 70$ and 84 mm) in the experiment [4] are taken as objects to

Table 1: Summary of t_a with different θ and t when T is 630 mm.

t (mm)	Additional thickness t_a (mm) with different inclined angle θ (°)										
	20°	22°	24°	26°	28°	30°	32°	34°	36°	38°	40°
60	14.2	14.6	15.1	15.5	15.9	16.2	16.6	16.9	17.3	17.6	18.0
70	15.2	15.7	16.2	16.6	17.1	17.4	17.8	18.2	18.6	18.9	19.3
80	16.1	16.6	17.1	17.6	18.0	18.4	18.8	19.2	19.6	20.0	20.4
90	16.8	17.4	17.9	18.4	18.8	19.3	19.7	20.1	20.5	20.9	21.3
100	17.4	18.0	18.5	19.1	19.5	20.0	20.4	20.8	21.2	21.6	22.0
110	17.9	18.5	19.1	19.6	20.1	20.6	21.0	21.4	21.9	22.3	22.7
120	18.4	19.0	19.6	20.1	20.6	21.1	21.5	22.0	22.4	22.8	23.2
130	18.8	19.4	20.0	20.6	21.1	21.5	22.0	22.4	22.9	23.3	23.7
140	19.1	19.8	20.4	20.9	21.5	21.9	22.4	22.9	23.3	23.7	24.2
150	19.4	20.1	20.7	21.3	21.8	22.3	22.8	23.2	23.7	24.1	24.6
160	19.7	20.4	21.0	21.6	22.1	22.6	23.1	23.6	24.0	24.5	24.9
170	19.9	20.6	21.2	21.8	22.4	22.9	23.4	23.9	24.3	24.8	25.2
180	20.1	20.8	21.5	22.1	22.6	23.2	23.7	24.1	24.6	25.1	25.5
190	20.3	21.0	21.7	22.3	22.9	23.4	23.9	24.4	24.9	25.3	25.8
200	20.5	21.2	21.9	22.5	23.1	23.6	24.1	24.6	25.1	25.6	26.0
210	20.7	21.4	22.1	22.7	23.3	23.8	24.3	24.8	25.3	25.8	26.2
220	20.8	21.6	22.2	22.9	23.5	24.0	24.5	25.0	25.5	26.0	26.4
230	21.0	21.7	22.4	23.0	23.6	24.2	24.7	25.2	25.7	26.2	26.6
240	21.1	21.9	22.5	23.2	23.8	24.3	24.8	25.4	25.9	26.3	26.8
250	21.2	22.0	22.7	23.3	23.9	24.5	25.0	25.5	26.0	26.5	27.0
260	21.3	22.1	22.8	23.5	24.0	24.6	25.1	25.6	26.2	26.6	27.1

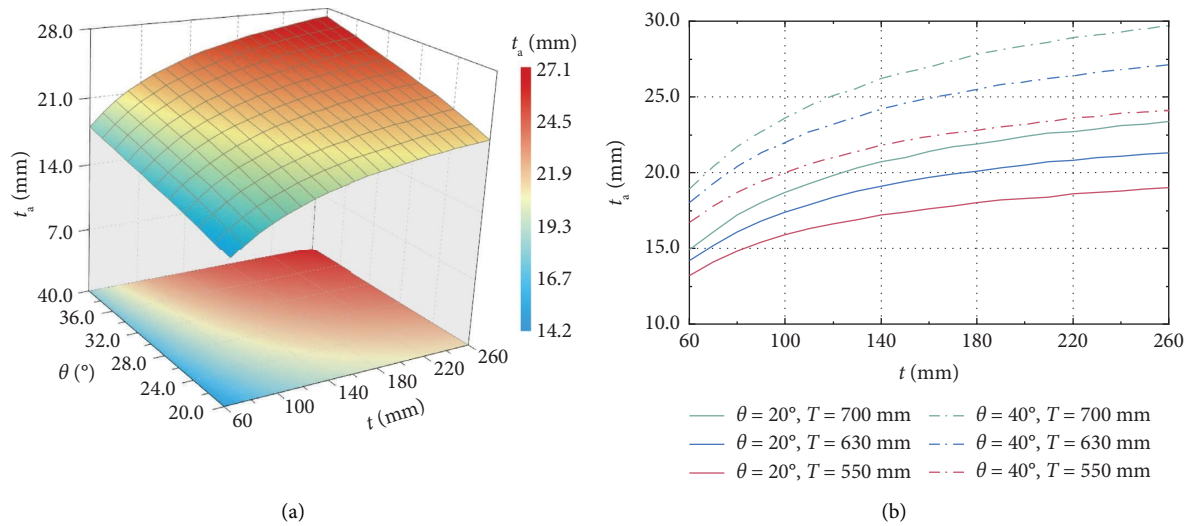

(a) (b)

Figure 3: The relationship among t_a, T, θ, and t. (a) The curved surface diagram of t_a varying with θ and t when T is 630 mm. (b) Curves of t_a varying with t when $\theta = 20$ and 40° and $T = 550$, 630, and 700 mm.

establish FE models. Furthermore, nonlinear analysis is performed in the ABAQUS/Standard analysis procedure to verify the applicability of the obtained equivalent thickness in RC stair slabs.

3.1. Solid Model Establishment. Figure 4(a) depicts the geometry and reinforcement of the stair slabs in the experiment [4]. The two stair slabs are placed parallel to the horizontal plane with a pin support at one end and a roller support at the other. The height and width of the steps are 155 and 260 mm, respectively. The used steel rebars with grade HPB300 represent the hot-rolled plain rebars with a yield strength of 300 MPa. However, the method of applying loads on the stair slabs is not described in detail for the experiment [4]. It is speculated that the loads might be imposed by putting mass blocks in the grooves between adjacent steps. Subsequently, these mass blocks could be simplified into the uniformly distributed line loads (denoted as p) positioned at the bottom edge of each groove, as shown in Figure 4(a).

The FE models of the stair slabs are illustrated in Figure 4(b). For the stair slabs with $t = 70$ and 84 mm, the respective equivalent thicknesses are 87 and 102 mm by equations (1)–(22). The FE models of the equivalent flat slabs are visualized in Figure 4(c). In the two types of models, the layout of longitudinal

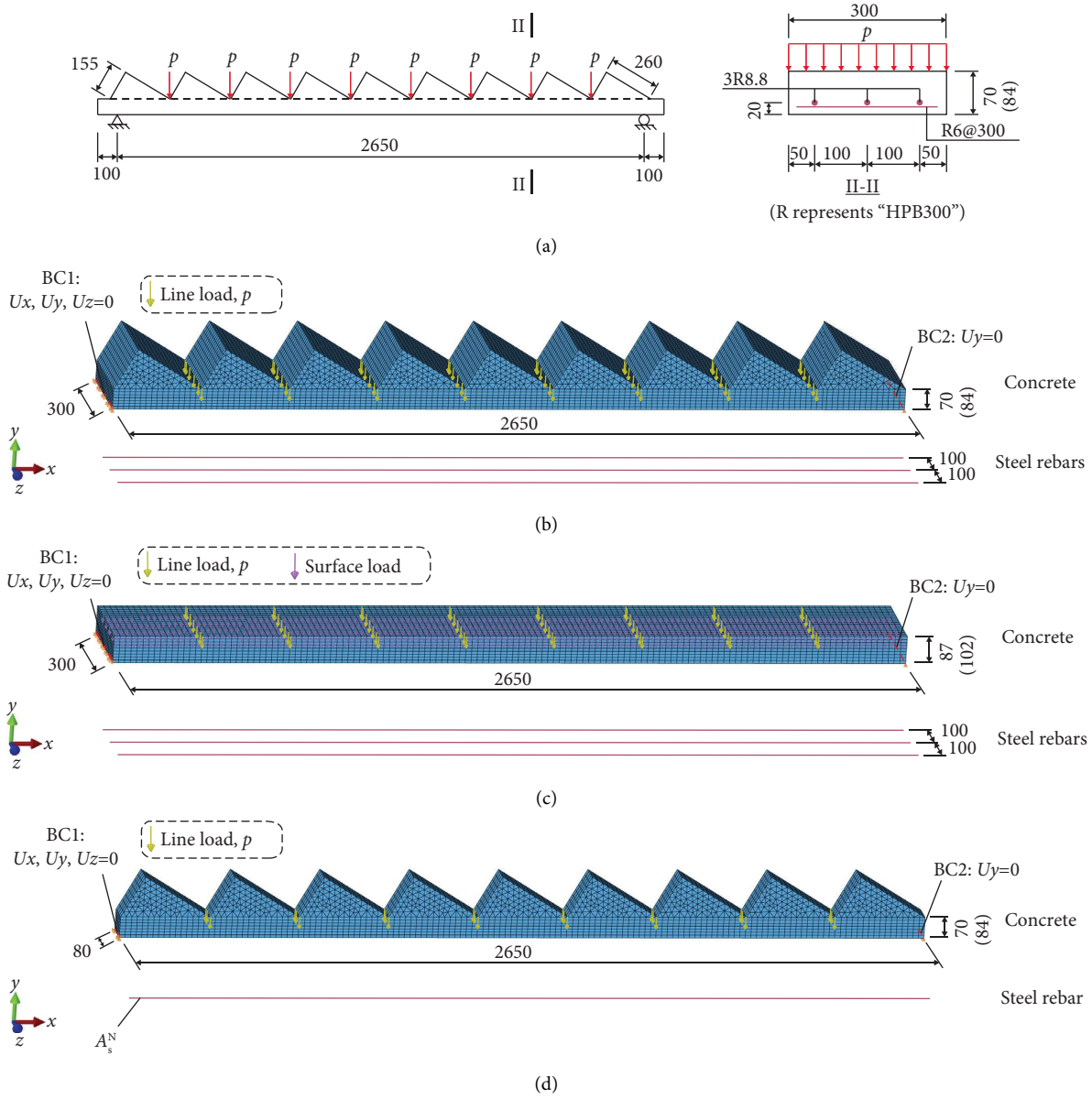

Figure 4: The configuration of the RC stair slabs in the experiment [4] and solid FE models including meshing, loads, and boundary conditions (unit: mm). (a) Geometry and reinforcement of the stair slabs in the experiment [4]. (b) Stair slab models. (c) Equivalent flat slab models. (d) Normalized models.

reinforcements is the same as that in Figure 4(a), whereas the distribution steel is ignored for simplicity.

For the sake of computational efficiency, the normalized models are introduced as shown in Figure 4(d). The normalized models are the stair slabs with a width of 80 mm, having only one longitudinal reinforcement. The area of the longitudinal reinforcement is defined as the normalized area A_s^N and written as follows:

$$A_s^N = \frac{20\pi D^2}{S}, \tag{25}$$

where D and S denote the diameter and spacing of the longitudinal reinforcements in the original stair slabs, respectively.

3.2. Element Types and Boundary Conditions. According to mesh size sensitivity analysis, appropriate element types and mesh sizes are selected for FE analysis in this study. The steps are discretized using six-node linear tetrahedral elements (C3D6) with a mesh size of 20 mm. Eight-node linear hexahedral elements (C3D8) are used to mesh the stair slabs excluding steps and the flat slabs, having mesh sizes of 20, 10, and 20 mm in the x, y, and z directions, respectively. The steel rebars are modeled using two-node linear truss

Table 2: Mechanical and physical properties of concrete and steel rebars.

Concrete		Steel rebar	
Cubic compressive strength, f_{cu} (MPa)	17*	Yield strength, f_y (MPa)	314*
Cylinder compressive strength, f_c (MPa)	12.92	Elastic modulus, E_s (GPa)	210
Tensile strength, f_t (MPa)	1.88	Poisson's ratio, ν_s	0.30
Elastic modulus, E_c (GPa)	23.58	Density, ρ_s (kg/m^3)	7850
Poisson's ratio, ν_c	0.20		
Density, ρ_c (kg/m^3)	2400		

Notes. *denotes the data measured in the experiment [4]; according to the Chinese code (GB 50010-2010) [29], $f_c = 0.76 f_{cu}$, $f_c = 0.395 f_{cu}^{0.55}$, and $E_c = 10^5/(2.2 + 34.7/f_{cu})$.

elements (T3D2) with a mesh size of 20 mm. The embedded region constraints are adopted to simulate the bonding between steel rebars and concrete, neglecting the relative slip of steel rebars to concrete.

The details relating to boundary conditions are given by BC1 and BC2 in Figures 4(b)–4(d). What is more, two analysis steps are created in these FE models. The gravity load is defined in the first analysis step. For the equivalent flat slab models, the gravity load is replaced by the uniformly distributed surface load to ensure that the gravity load in the flat slab models is the same as that in the stair slab models. The surface loads are taken as 3.28 and 3.61 kN/m^2 when $t = 70$ and 84 mm, respectively. In the second analysis step, the uniformly distributed line loads (p) are applied to the FE models.

3.3. Material Properties. The mechanical and physical properties of concrete and steel rebars are listed in Table 2.

The concrete damaged plasticity (CDP) model [31, 32] accurately describes the main failure mechanisms of concrete (i.e., compressive crushing [33] and tensile cracking), having widespread application in FE simulation of various members such as slabs [34], columns [35], walls [36, 37], and joints [38, 39]. The mechanical behavior of concrete requires to be defined in the CDP model, including plastic behavior, compressive behavior, and tensile behavior.

For plastic behavior of concrete, basic parameters and their values are as follows: the dilation angle $\Phi = 30^\circ$, the plastic potential eccentricity $\delta = 0.1$ [40], the ratio of strength in biaxial compression to uniaxial compression $f_b/f_c = 1.16$ [40], the ratio of the second stress invariant on the tensile meridian to that on the compressive meridian $K_c = 2/3$ [40], and the viscosity parameter $\mu = 0.0025$.

In addition, compressive behavior and tensile behavior are determined by the uniaxial stress-strain relationship of concrete, as shown in Figure 5.

Figure 5(a) illustrates the uniaxial compressive stress-strain ($\sigma_c - \varepsilon_c$) curve of concrete, which is expressed as follows [29]:

$$\sigma_c = \begin{cases} \dfrac{f_c E_c \varepsilon_c}{f_c + \left(\varepsilon_c/\varepsilon_{cp}\right)^n \left(E_c \varepsilon_{cp} - f_c\right)}, & \varepsilon_c \le \varepsilon_{cp}, \\ \dfrac{f_c\left(\varepsilon_c/\varepsilon_{cp}\right)}{\alpha_c\left[\left(\varepsilon_c/\varepsilon_{cp}\right) - 1\right]^2 + \left(\varepsilon_c/\varepsilon_{cp}\right)}, & \varepsilon_c > \varepsilon_{cp}, \end{cases} \tag{26}$$

where ε_{cp} is the peak strain of concrete in compression and α_c is the descending segment parameter in the compressive stress-strain curve of concrete. The ε_{cp} and α_c are obtained as follows [29]:

$$\varepsilon_{cp} = \left(700 + 172\sqrt{f_c}\right) \times 10^{-6}, \qquad \alpha_c = 0.157 f_c^{0.785} - 0.905. \tag{27}$$

Figure 5(b) depicts the uniaxial tensile stress-strain (σ_t–ε_t) curve of concrete, which is written as follows [29]:

$$\sigma_t = \begin{cases} f_t\left[1.2\left(\dfrac{\varepsilon_t}{\varepsilon_{tp}}\right) - 0.2\left(\dfrac{\varepsilon_t}{\varepsilon_{tp}}\right)^6\right], & \varepsilon_t \le \varepsilon_{tp}. \\ \dfrac{f_t\left(\varepsilon_t/\varepsilon_{tp}\right)}{\alpha_t\left[\left(\varepsilon_t/\varepsilon_{tp}\right) - 1\right]^{1.7} + \left(\varepsilon_t/\varepsilon_{tp}\right)}, & \varepsilon_t > \varepsilon_{tp}, \end{cases} \tag{28}$$

where ε_{tp} is the peak strain of concrete in tension and α_t is the descending segment parameter in the tensile stress-strain curve of concrete. The ε_{tp} and α_t are represented as follows [29]:

$$\varepsilon_{tp} = f_t^{0.54} \times 65 \times 10^{-6}, \qquad \alpha_t = 0.312 f_t^2. \tag{29}$$

In ABAQUS, the concrete compression hardening data are defined by the inelastic strain ε_c^{in}, and the concrete tension stiffening data are given by the cracking strain ε_t^{ck}. The ε_c^{in} and ε_t^{ck} are formulated as follows [40]:

$$\varepsilon_c^{in} = \varepsilon_c - \frac{\sigma_c}{E_c}, \qquad \varepsilon_t^{ck} = \varepsilon_t - \frac{\sigma_t}{E_c}. \tag{30}$$

For steel rebars, the constitutive relationship is assumed to be an ideal elastoplastic model. In other words, the stress is initially proportional to the strain, but the stress remains the same with the increase of the strain after steel rebars yield.

3.4. Results and Validation. For the stair slabs with $t = 70$ and 84 mm, Figure 6 compares the load-displacement curves in the experimental results [4] and the simulation results. The values of the maximum deflection Δ_G due to gravity are detailed in legends. It is noted that the horizontal axis in

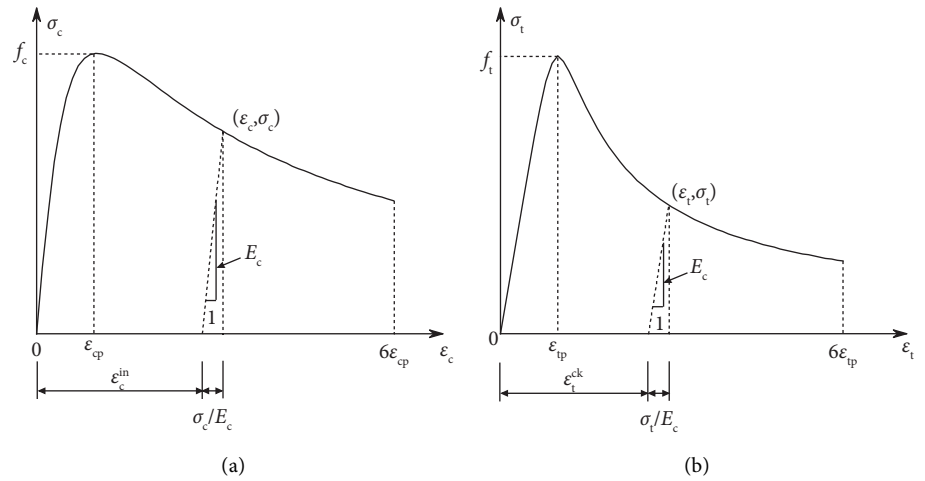

Figure 5: The uniaxial stress-strain relationship of concrete. (a) Compression. (b) Tension.

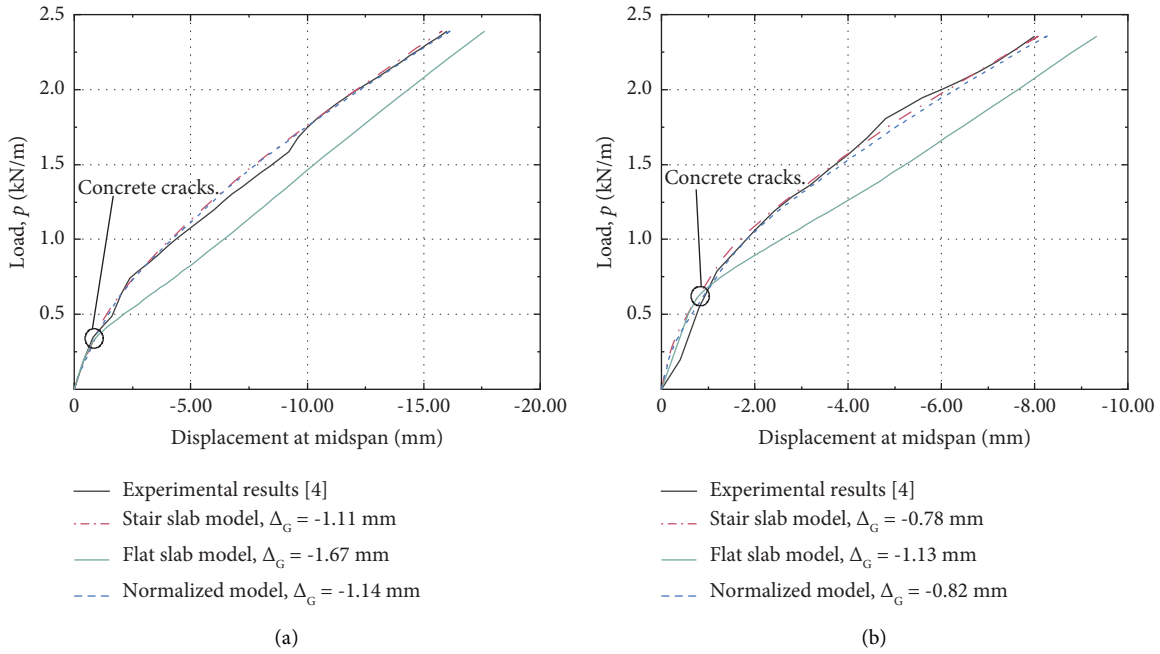

Figure 6: Load-displacement curves in the experimental results [4] and the simulation results for the stair slabs with different thicknesses. (a) $t = 70$ mm. (b) $t = 84$ mm.

Figure 6 denotes the displacement at midspan due to the line loads p, not containing the Δ_G. Subsequently, taking the stair slab with $t = 84$ mm as the object, it is assumed that the maximum moment (taken as 0.96 kN·m) under gravity is imposed on the unit cell at midspan. Then, equations (1)–(19) can be used to derive the theoretical results of the normal stress distribution in the unit cell. For the unit cell at midspan, Figure 7 compares the normal stress distributions due to gravity in the simulation results and the theoretical results.

In Figures 6(a) and 6(b), the simulation results of the stair slab models are in good agreement with the experimental results [4], and most of the deviations are less than 10%. It means that the chosen constitutive models and material parameters are reasonable in this study. On the other hand, it can be observed that the initial stiffness of the equivalent flat slab models is close to that of the stair slab models. This implies that the obtained equivalent thickness can be reliably applied in RC stair slabs within the elastic range. However, the deformation of the flat slab models is significantly larger than that of the stair slab models after concrete cracking. The reason might be attributed to the difference in damage development between the flat slabs and the stair slabs. In the flat slabs, the curvature at the midspan increases rapidly due to cracking, leading to a sharp reduction of the overall stiffness. In the stair slabs, initial cracks might simultaneously occur at several cross sections with the minimum depth around the midspan so that the curvatures

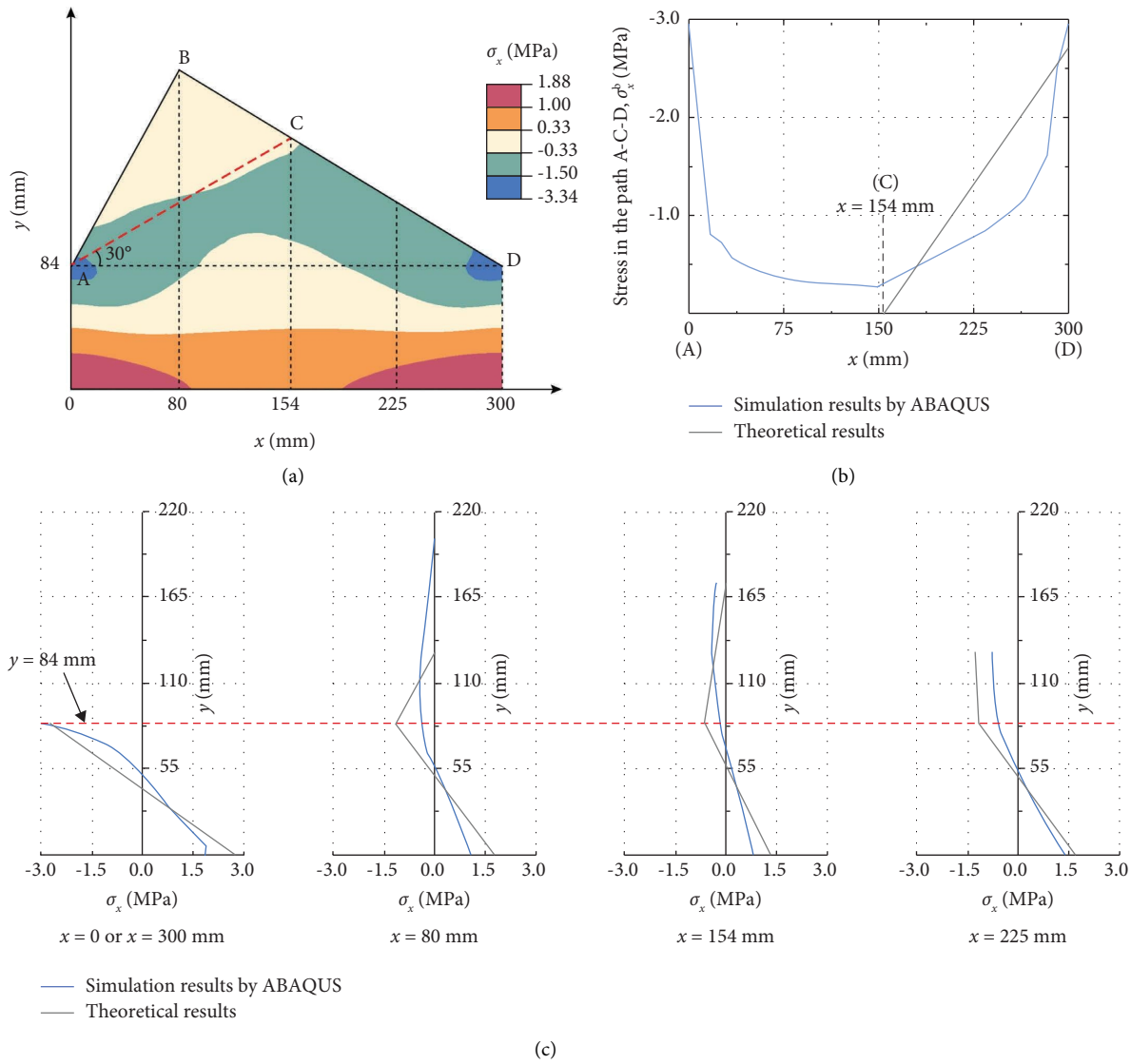

FIGURE 7: The normal stress distributions due to gravity in the simulation results and the theoretical results for the unit cell at midspan of the stair slab with $t = 84$ mm. (a) The stress contour in the simulation results. (b) Comparison of the stresses in the path A–C-D. (c) Comparison of the stresses at $x = 0$ or 300, 80, 154, and 225 mm.

at these cross sections increase slowly to alleviate the decline of the overall stiffness. Besides, the discrepancy in the simulation results between the normalized models and the stair slab models is very small. In terms of the computation time, the former is about one-seventh of the latter. Thus, the stair slab models can be substituted with the normalized models to improve computational efficiency for further analysis.

For the stress contour in Figure 7(a), it is assumed that the regions where the magnitude of stress does not exceed 0.33 MPa (i.e., one-tenth of the magnitude of the maximum compressive stress) are defined as the regions with small stresses. These regions exist near the neutral surface and the part ABC of the step. For the stresses in the path A-C-D in Figure 7(b), the stress distributions in the simulation results and the theoretical results are similar. Still, they have evident differences because of the stress concentrations around points A and D. On each section in Figure 7(c), it can be seen that the location of the neutral axis in the simulation results is generally higher than that in the theoretical results. On the tension zone, the stresses in both the simulation results and the theoretical results are approximately proportional to the distance from the neutral axis. On the compression zone, the stress distribution is nonlinear in the simulation results but linear or bilinear in the theoretical results. As can be observed from Figures 7(b) and 7(c), the theoretical results are larger than the simulation results in most cases, causing the overestimation of the calculated bending strain energy by equation (20). Afterwards, it is confirmed from equation (22) that the obtained equivalent thickness is slightly conservative so that the overall stiffness of stair slabs is underestimated. This can explain why the values of the Δ_G in

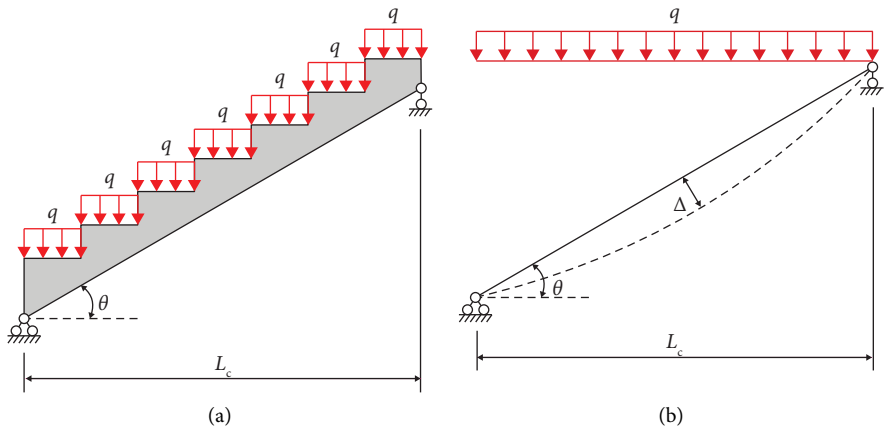

FIGURE 8: The simplified stair slab model during design. (a) The uniformly distributed loads on the treads of the stair slab. (b) The simply supported beam model.

the flat slab models are larger than those in the stair slab models in Figure 6.

It can be concluded that there are two main sources of errors when the stair slabs are equivalent to the flat slabs. One is that the errors between the assumed stresses and their actual values in the unit cell within the elastic range, and the other is the difference in damage development between the stair slabs and the flat slabs after concrete cracking.

4. Proposed Design Method for Stair Slabs considering Step Stiffness

In engineering practice, RC stair slabs are sloped to make all treads parallel to the horizontal plane. During design, the uniformly distributed loads (denoted as q) are imposed perpendicular to treads, as shown in Figure 8(a). If the negative moments at supports are neglected, the stair slab can be regarded as a simply supported beam in Figure 8(b). In the following, the design process of stair slabs considering step stiffness is presented based on two design codes of China, i.e., the Load Code for the Design of Building (GB 50009-2012) [28] and the Code for Design of Concrete Structures (GB 50010-2010) [29].

The thickness t of stair slabs can be initially estimated as follows:

$$t = \max\left\{10 \times \text{floor}\left(\frac{L_c}{300}\right), 80\,\text{mm}\right\}, \tag{31}$$

where floor(x) denotes the rounding function that decreases a given number x to the next highest integer and L_c is the clear span of stair slabs. The unit of L_c in equation (31) is mm.

The load q consists of the dead load q_D and the live load q_L. The dead load q_D is expressed as follows:

$$q_D = q_G + q_a, \tag{32}$$

where q_G denotes the gravity load, and q_a denotes the additional load (e.g., the handrail load, the surface layer load, and the mortar load). The gravity load q_G can be calculated as follows:

$$q_G = \left(\frac{h}{2} + \frac{\text{st}}{b}\right)\rho_c g_G, \tag{33}$$

where g_G is the acceleration of gravity usually taken as 9.8 m/s^2.

For strength design, the thickness t is used because the strength of stair slabs is determined by the bearing capacity of the cross sections with the minimum depth. Based on the fundamental combination of loads [28], the maximum bending moment M_S at midspan is obtained as follows:

$$M_s = 0.125\left(\gamma_D q_D + \gamma_L q_L\right) w L_c^2, \tag{34}$$

where γ_D and γ_L are the partial factors of the dead load and the live load, respectively.

After that, the required steel area A_s in the stair slab with the width w is derived as follows [29]:

$$A_s = \max\left\{\xi w\left(t - c_s\right)\frac{\alpha_1 f_c}{f_y}, \rho_{\min} w t\right\}, \tag{35}$$

where ξ is the relative height of the compression zone, α_1 is the ratio of the average stress on the compression zone to the cylinder compressive strength of concrete, c_s is the distance from the center of longitudinal reinforcements to the bottom of the stair slab, and $\rho_{\min}$ is the minimum reinforcement ratio. ξ is formulated as follows [29]:

$$\xi = 1 - \sqrt{1 - \frac{2M_S}{\alpha_1 f_c w\left(t - c_s\right)^2}}. \tag{36}$$

To avoid the crushing of the concrete on the compression zone before the longitudinal tension reinforcement yield, the following inequality should be satisfied [29]:

$$A_s \le \xi_b w\left(t - a_s\right)\frac{\alpha_1 f_c}{f_y}, \tag{37}$$

where ξ_b is the relative height limit of the compression zone.

For the deflection calculation, the equivalent thickness t_e is adopted to consider the beneficial influence of steps on the overall stiffness of stair slabs. Based on the quasi-permanent

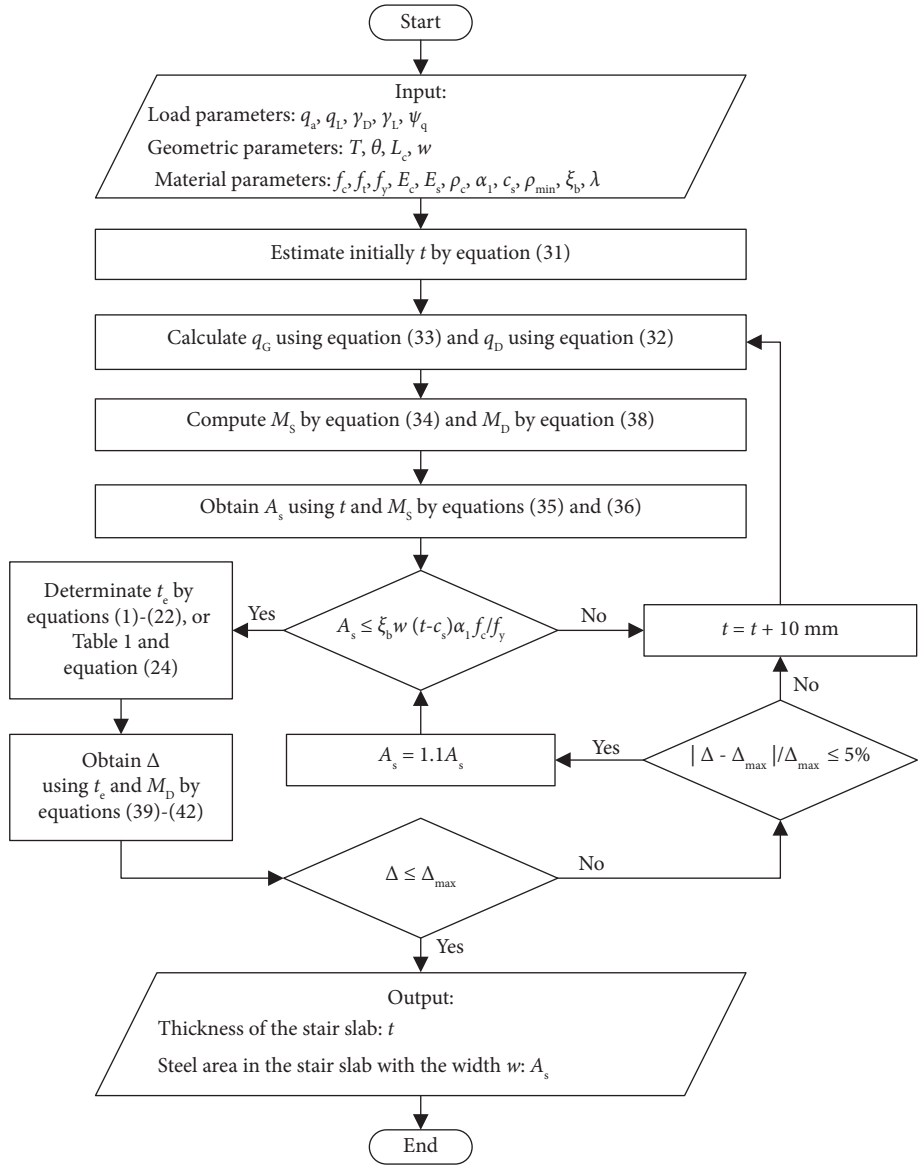

Figure 9: The flow chart of the design method considering step stiffness for RC stair slabs based on the Chinese codes [28, 29].

combination of loads [28], the maximum bending moment M_D at midspan is computed as follows:

$$M_D = 0.125\left(q_D + \psi_q q_L\right) w L_c^2, \tag{38}$$

where ψ_q is the coefficient of the quasi-permanent value for the live load.

Subsequently, the short-term stiffness B_s of stair slabs is expressed as follows [29]:

$$B_s = \frac{E_s A_s \left(t_e - c_s\right)^2}{1.15\psi + 0.2 + \left(6A_s E_s / w\left(t_e - c_s\right) E_c\right)}, \tag{39}$$

where ψ denotes the strain nonuniformity coefficient of the longitudinal tension reinforcements between cracks. ψ is written as follows [29]:

$$\psi = \min\left\{\max\left\{1.1 - \frac{0.4 w t_e \left(t_e - c_s\right) f_t}{M_D}, 0.2\right\}, 1.0\right\}. \tag{40}$$

Correspondingly, the short-term deflection Δ_s at midspan is given as follows:

$$\Delta_s = \frac{5 M_D L_c^2}{48 B_s \cos^2\theta}. \tag{41}$$

Under sustained loads, the deflection of stair slabs can significantly increase due to the creep and shrinkage of concrete. The Chinese design code [29] specifies a deflection magnification factor to consider the combined effects of creep and shrinkage for flexural members under long-term loads. Thus, the long-term deflection Δ at midspan of stair slabs can be represented as follows:

Table 3: Design parameters for RC stair slabs.

Type	Parameters
Load parameters	$q_a = 2.5\ \text{kN/m}^2$, $\gamma_D = 1.3$, $\gamma_L = 1.5$, and $\psi_q = 0.3$
Geometric parameters	$T = 630\ \text{mm}$ and $\omega = 1000\ \text{mm}$
Material parameters	$f_c = 14.3\ \text{N/mm}^2$, $f_t = 1.43\ \text{N/mm}^2$, $f_y = 360\ \text{N/mm}^2$, $E_c = 30\ \text{GPa}$, $E_s = 200\ \text{GPa}$, $\rho_c = 2400\ \text{kg/m}^3$, $\alpha_1 = 1.0$, $c_s = 25\ \text{mm}$, $\rho_{\min} = 0.2\%$, $\xi_b = 0.5176$, and $\lambda = 2.0$

Table 4: The required thickness and the steel area in the stair slabs.

θ (°)	L_c (mm)	$q_L = 2\ \text{kN/m}^2$		$q_L = 3.5\ \text{kN/m}^2$		$q_L = 5\ \text{kN/m}^2$	
		t (mm)	A_s (mm^2)	t (mm)	A_s (mm^2)	t (mm)	A_s (mm^2)
25	3910	140	662	140	785	140	913
	4560	170	763	170	894	160	1211
	4890	180	926	180	984	180	1129
	5540	210	1062	210	1228	210	1271
	5870	230	1017	230	1168	220	1519
30	4090	150	707	150	830	150	958
	4380	160	847	160	901	160	1037
	4960	190	861	190	997	190	1136
	5550	220	971	220	1114	220	1260
	6130	250	1199	250	1240	240	1590
35	3930	150	675	150	788	140	1080
	4450	170	862	170	909	170	1037
	4980	200	867	200	995	190	1303
	5500	230	961	220	1248	220	1406
	6030	250	1210	250	1369	250	1393

$$\Delta = \lambda \Delta_s, \tag{42}$$

where λ denotes the deflection magnification factor and is taken as 2.0 when no reinforcement is provided on the compression side of stair slabs [29].

When the clear span L_c is less than 7 m, the maximum permissible deflection $\Delta_{\max}$ of stair slabs is defined as follows [29]:

$$\Delta_{\max} = \frac{L_c}{200 \cos \theta}. \tag{43}$$

Based on the Chinese codes [28, 29], Figure 9 shows the flow chart of the design method considering step stiffness for RC stair slabs.

5. Assessment of the Proposed Design Method

In this section, several numerical examples are presented to illustrate the reliability and advantages of the proposed design method in comparison with the FE method and the conventional method. The design parameters in Table 3 are used in all examples.

In the FE method, the normalized models are adopted to perform nonlinear analysis in the ABAQUS/Standard analysis procedure. The parameters in the CDP model, including Φ, δ, f_b/f_c, K_c, and μ, are identical to those used in Section 3.3. Different from the modeling method demonstrated in Figure 4(d), only one analysis step needs to be created for these models. In the analysis step, the uniformly distributed loads based on the quasi-permanent combination [28] are perpendicularly imposed on all treads, as depicted in Figure 8(a). In addition, the normalized area A_s^N is taken as $80A_s/w$ in these models. The conventional method is obtained by substituting t_e in Figure 9 by t, ignoring the effect of step stiffness. In the conventional method, it is suggested that the expression $|\Delta - \Delta_{\max}|/\Delta_{\max}$ is set to no more than 50% to ensure that the thickness and the reinforcement ratio of stair slabs are economical and practical. In this study, the proposed design method and the conventional method were implemented in MATLAB.

5.1. Comparison between the Proposed Design Method and the FE Method. According to the proposed design method, the required thickness and steel area in the stair slabs are tabulated in Table 4. During the design process of these examples, the values of the short-term deflection Δ_s can be given by equation (41). It should be noted that the results in Table 4 are also used to establish the normalized models. By the FE method, the derived displacement at midspan is denoted as the short-term deflection Δ_{sFEM}. Table 5 compares the short-term deflection at midspan in the design results (Δ_s) and the simulation results (Δ_{sFEM}). The scatter plot in Figure 10 visualizes the relationship between the design results (Δ_s) and the simulation results (Δ_{sFEM}). The simulation results consider the plastic behavior of concrete and are approximate to the actual instantaneous deflection of stair slabs to a certain extent. The ratio of the Δ_s to the Δ_{sFEM}, denoted as n, can represent the accuracy of the design results. The closer the value of n is to 1.0, the more accurate

Table 5: The short-term deflection at midspan in the design results (Δ_s) and the simulation results (Δ_{sFEM}).

θ (°)	L_c (mm)	$q_L = 2$ kN/m^2			$q_L = 3.5$ kN/m^2			$q_L = 5$ kN/m^2		
		Δ_s (mm)	Δ_{sFEM} (mm)	n	Δ_s (mm)	Δ_{sFEM} (mm)	n	Δ_s (mm)	Δ_{sFEM} (mm)	n
25	3910	10.1	4.7	2.1	9.9	4.9	2.0	9.7	5.2	1.9
	4560	11.7	6.4	1.8	11.5	6.6	1.7	12.1	7.8	1.6
	4890	12.8	7.5	1.7	13.3	8.3	1.6	13.0	8.5	1.5
	5540	14.7	9.8	1.5	14.3	9.9	1.4	15.0	10.6	1.4
	5870	16.2	10.8	1.5	15.7	10.9	1.4	15.7	11.5	1.4
30	4090	11.4	5.8	2.0	11.1	6.0	1.9	11.0	6.3	1.7
	4380	12.1	6.7	1.8	12.6	7.4	1.7	12.4	7.6	1.6
	4960	14.2	8.6	1.7	13.9	8.9	1.6	13.6	9.1	1.5
	5550	16.0	10.4	1.5	15.5	10.6	1.5	15.2	10.7	1.4
	6130	16.6	11.7	1.4	17.3	12.4	1.4	17.2	13.1	1.3
35	3930	10.9	5.2	2.1	10.7	5.6	1.9	11.7	6.9	1.7
	4450	12.7	7.3	1.7	13.3	8.0	1.7	13.0	8.2	1.6
	4980	14.6	8.8	1.7	14.3	9.0	1.6	14.8	10.2	1.5
	5500	15.9	10.0	1.6	16.0	11.2	1.4	15.7	11.3	1.4
	6030	17.9	12.4	1.4	17.4	12.5	1.4	18.3	13.4	1.4

Note. $n = \Delta_s/\Delta_{sFEM}$.

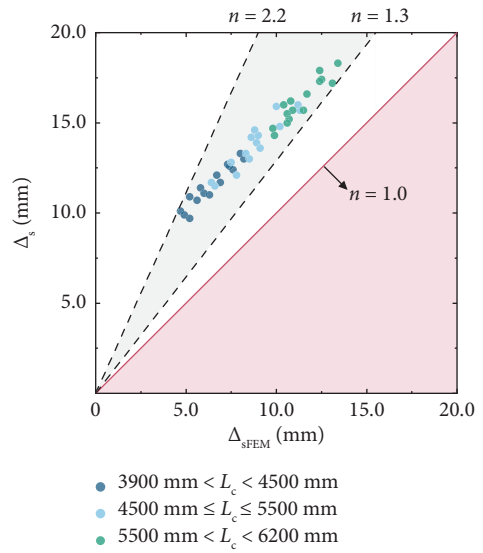

Figure 10: The scatter plot between the design results (Δ_s) and the simulation results (Δ_{sFEM}).

Table 6: The required thickness and the steel area in the stair slabs when $\theta = 30°$.

L_c (mm)	Proposed design method						Conventional method					
	$q_L = 2$ kN/m^2		$q_L = 3.5$ kN/m^2		$q_L = 5$ kN/m^2		$q_L = 2$ kN/m^2		$q_L = 3.5$ kN/m^2		$q_L = 5$ kN/m^2	
	t (mm)	A_s (mm^2)	t (mm)	A_s (mm^2)	t (mm)	A_s (mm^2)	t (mm)	A_s (mm^2)	t (mm)	A_s (mm^2)	t (mm)	A_s (mm^2)
4090	150	707	150	830	150	958	170	920	170	972	170	1111
4380	160	847	160	901	160	1037	180	1012	180	1173	180	1338
4960	190	861	190	997	190	1136	210	1161	210	1212	210	1371
5550	220	971	220	1114	220	1260	240	1210	240	1378	230	1770
6130	250	1199	250	1240	240	1590	270	1375	270	1554	260	1972

the design results. Notice that the structural safety requires that the value of n should not be less than 1.0.

In Table 4, the thickness t and the steel area A_s increase with the growth of the clear span L_c. As the live load q_L rises, the steel area A_s grows, whereas the thickness t might decrease in some situations. That is because the relatively thin stair slabs require more steel area during strength design, contributing to controlling deflection to some extent.

As can be seen from Table 5 and Figure 10, when the clear span L_c is in the range of 3900 to 6200 mm, the ratio n varies from 1.3 to 2.2 and tends to decrease as the L_c increases. The results demonstrate that the proposed design method is reliable and can assure the safe performance of RC stair slabs. And the calculated deflection has higher accuracy with the growth of the clear span L_c. Despite this, there exist two sources of errors in the proposed design method. One is that the Chinese design code [29] specifies the minimum stiffness at cracking cross sections as the overall stiffness to compute deflection, neglecting the stiffness variation along the stair slab span; the other is that the difference in damage development between flat slabs and stair slabs after concrete cracking is not considered in the design process.

Consequently, to further improve the accuracy of the new deflection calculation method, some effective measures should be taken, including perfecting the assumption of the stress distribution in a unit cell and considering the characteristic of the stiffness variation and the damage development for stair slabs in the design process.

5.2. Comparison between the Proposed Design Method and the Conventional Method. Based on the proposed design method and the conventional method, Table 6 lists the required thickness t and steel area A_s in the stair slabs when $\theta = 30^\circ$. Compared with the conventional method, the steel area A_s drops by 12 to 26 percent while the thickness t is reduced by 10 to 20 mm in the proposed design method. It is concluded that the proposed design method can decrease the consumption of concrete and steel.

6. Conclusions and Outlook

In this article, the equivalent thickness of stair slabs is derived theoretically and verified by nonlinear analysis. For reinforced concrete (RC) stair slabs, a novel design method considering step stiffness is proposed. Subsequently, several numerical examples are presented to illustrate the reliability and advantages of the proposed design method. The main conclusions are drawn as follows:

(1) The equivalent thickness only depends on the characteristic length of steps, the inclined angle of stair slabs, and the thickness of stair slabs. The larger these parameters are, the more contribution the steps make to the stiffness of the stair slabs.

(2) The obtained equivalent thickness is slightly conservative and can be reliably applied to RC stair slabs within the elastic range. After concrete cracking, the deformation of the equivalent flat slabs is larger than that of stair slabs due to the difference in damage development. The stair slab models can be substituted with the normalized models to improve computational efficiency.

(3) Compared with the finite element method and the conventional method, the design method considering step stiffness can not only ensure structural safety for RC stair slabs but also decrease the consumption of concrete and steel.

This article provides a simple and efficient way to evaluate the stiffness of RC stair slabs and calculate their deflections. The proposed design method can help engineers in design offices optimize the thickness of stair slabs, achieve the lightweight design of stairs, and solve headroom problems possibly occurring at staircases. Moreover, the method contributes to saving building costs and could be applied to the safety assessment of existing stair structures. Future studies will further improve the accuracy of this deflection calculation method by more exact assumption of the stress distribution in a unit cell and more full consideration of the stiffness variation and the damage development for stair slabs.

Data Availability

The data used to support the findings of this study are included within the article.

Conflicts of Interest

The authors declare that there are no conflicts of interest.

References

[1] Z. Mohammad, S. M. Talha, and A. Baqi, "Seismic performance of stairs as isolated and built-in RC frame building," *Advances in Structural Engineering: Dynamics*, Springer India, New Delhi, India, 2015.

[2] D. Menon, K. V. Sivaraman, and M. Janardhana, "Improved codal recommendations for design of RC dog-legged stairs supported on transverse landing edges," *Journal of Structural Engineering*, vol. 37, no. 5, pp. 342–346, 2010.

[3] P. Halpin and A. Mannis, "Projects in belfast and dublin," *Structural Engineer*, vol. 87, no. 8, pp. 13-14, 2009.

[4] J. Xiong, W. Cheng, K. Zhou, and G. Gui, "Calculation of deformation of reinforced concrete plate stairs," *Building Structure*, vol. 31, no. 5, pp. 26–28, 2001.

[5] Z. Friedman and J. B. Kosmatka, "Exact stiffness matrix of a nonuniform beam—I. Extension, torsion, and bending of a Bernoulli-Euler beam," *Computers and Structures*, vol. 42, no. 5, pp. 671–682, 1992.

[6] Z. Friedman and J. B. Kosmatka, "Exact stiffness matrix of a nonuniform beam—II. Bending of a Timoshenko beam," *Computers and Structures*, vol. 49, no. 3, pp. 545–555, 1993.

[7] A. Tena-Colunga, "Stiffness formulation for nonprismatic beam elements," *Journal of Structural Engineering*, vol. 122, no. 12, pp. 1484–1489, 1996.

[8] C. Franciosi and M. Mecca, "Some finite elements for the static analysis of beams with varying cross section," *Computers and Structures*, vol. 69, no. 2, pp. 191–196, 1998.

[9] S. Li, J. Hu, C. Zhai, and L. Xie, "A unified method for modeling of axially and/or transversally functionally graded beams with variable cross-section profile," *Mechanics Based Design of Structures and Machines*, vol. 41, no. 2, pp. 168–188, 2013.

[10] F. Romano, "Deflections of Timoshenko beam with varying cross-section," *International Journal of Mechanical Sciences*, vol. 38, no. 8-9, pp. 1017–1035, 1996.

[11] K. Yoon and P.-S. Lee, "Modeling the warping displacements for discontinuously varying arbitrary cross-section beams," *Computers and Structures*, vol. 131, pp. 56–69, 2014.

[12] Z. Huang, Y. Xing, and Y. Gao, "A new method of stiffness prediction for periodic beam-like structures," *Composite Structures*, vol. 267, Article ID 113892, 2021.

[13] J. W. Jaworski and E. H. Dowell, "Free vibration of a cantilevered beam with multiple steps: comparison of several theoretical methods with experiment," *Journal of Sound and Vibration*, vol. 312, no. 4-5, pp. 713–725, 2008.

[14] A. A. Diwan, L. S. Al-Ansari, A. A. Al-Saffar, and Q. S. Al-Anssari, "Experimental and theoretical investigation of static deflection and natural frequency of stepped cantilever beam," *Australian Journal of Mechanical Engineering*, vol. 20, no. 2, pp. 303–315, 2022.

[15] S. Kukla and I. Zamojska, "Frequency analysis of axially loaded stepped beams by Green's function method," *Journal of Sound and Vibration*, vol. 300, no. 3–5, pp. 1034–1041, 2007.

[16] Z. R. Lu, M. Huang, J. K. Liu, W. Chen, and W. Liao, "Vibration analysis of multiple-stepped beams with the composite element model," *Journal of Sound and Vibration*, vol. 322, no. 4-5, pp. 1070–1080, 2009.

[17] Q. Mao, "Free vibration analysis of multiple-stepped beams by using Adomian decomposition method," *Mathematical and Computer Modelling*, vol. 54, no. 1-2, pp. 756–764, 2011.

[18] X. Wang and Y. Wang, "Free vibration analysis of multiple-stepped beams by the differential quadrature element method," *Applied Mathematics and Computation*, vol. 219, no. 11, pp. 5802–5810, 2013.

[19] G. Duan and X. Wang, "Free vibration analysis of multiple-stepped beams by the discrete singular convolution," *Applied Mathematics and Computation*, vol. 219, no. 24, pp. 11096–11109, 2013.

[20] R. M. Lin and T. Y. Ng, "Exact vibration modes of multiple-stepped beams with arbitrary steps and supports using elemental impedance method," *Engineering Structures*, vol. 152, pp. 24–34, 2017.

[21] N. El-Mezaini, C. Balkaya, and E. Çitipitiolu, "Analysis of frames with nonprismatic members," *Journal of Structural Engineering*, vol. 117, no. 6, pp. 1573–1592, 1991.

[22] T. Zheng and T. Ji, "Equivalent representations of beams with periodically variable cross-sections," *Engineering Structures*, vol. 33, no. 3, pp. 706–719, 2011.

[23] T. Zheng and T. Ji, "An approximate method for determining the static deflection and natural frequency of a cracked beam," *Journal of Sound and Vibration*, vol. 331, no. 11, pp. 2654–2670, 2012.

[24] X. Xu, "Deflection calculation and design suggestions for reinforced concrete slab stairs considering the effect of steps," *Building Structure*, vol. 50, no. 13, pp. 30–37, 2020.

[25] S. Yi, L. Xu, G. Cheng, and Y. Cai, "FEM formulation of homogenization method for effective properties of periodic heterogeneous beam and size effect of basic cell in thickness direction," *Computers and Structures*, vol. 156, pp. 1–11, 2015.

[26] S. Yi, G. Cheng, and L. Xu, "Stiffness design of heterogeneous periodic beam by topology optimization with integration of commercial software," *Computers and Structures*, vol. 172, pp. 71–80, 2016.

[27] L. Xu and Z. Qian, "Microstructural topology optimization of periodic beam structures based on the relaxed Saint-Venant solution," *Structural and Multidisciplinary Optimization*, vol. 63, no. 4, pp. 1813–1837, 2021.

[28] Ministry of Housing and Urban-Rural Construction of the People's Republic of China, *Load Code for the Design of Building Structures: GB 50009-2012*, China Architecture and Building Press, Beijing, China, 2012.

[29] Ministry of Housing and Urban-Rural Construction of the People's Republic of China, *Code for Design of concrete Structures: GB 50010-2010*, China Architecture and Building Press, Beijing, China, 2015.

[30] W. Mannes, *Techniques of Staircase Construction: Technical and Design Instructions for Stairs Made of wood, Steel, concrete, and Natural Stone*, Springer Press, New York, NY, USA, 1979.

[31] J. Lubliner, J. Oliver, S. Oller, and E. Oñate, "A plastic-damage model for concrete," *International Journal of Solids and Structures*, vol. 25, no. 3, pp. 299–326, 1989.

[32] J. Lee and G. L. Fenves, "Plastic-damage model for cyclic loading of concrete structures," *Journal of Engineering Mechanics*, vol. 124, no. 8, pp. 892–900, 1998.

[33] E. Mansouri, M. Manfredi, and J.-W. Hu, "Environmentally friendly concrete compressive strength prediction using hybrid machine learning," *Sustainability*, vol. 14, no. 20, Article ID 12990, 2022.

[34] E. S. Kalib and Y. W. Shewalul, "Response of the flat reinforced concrete floor slab with openings under cyclic in-plane loading," *Advances in Civil Engineering*, vol. 20219 pages, Article ID 2503475, 2021.

[35] A. Raza, Q. U. Z. Khan, and A. Ahmad, "Numerical investigation of load-carrying capacity of GFRP-reinforced rectangular concrete members using CDP model in ABAQUS," *Advances in Civil Engineering*, vol. 2019, Article ID 1745341, 21 pages, 2019.

[36] K. Ma, Y. Ma, and B. Liu, "Quasistatic cyclic tests and finite element analysis of low-aspect ratio double steel concrete composite walls," *Advances in Civil Engineering*, vol. 2019, Article ID 5917380, 12 pages, 2019.

[37] Z. Zhou, J. Qian, and W. Huang, "Numerical study on deformation capacity of steel plate reinforced concrete shear walls," *Advances in Civil Engineering*, vol. 2019, Article ID 9701324, 13 pages, 2019.

[38] G. Kenea and A. Feyissa, "Cyclic behavior of reinforced concrete slab-column connection using numerical simulation," *Advances in Civil Engineering*, vol. 2022, Article ID 2814715, 14 pages, 2022.

[39] A. Hamicha and G. Kenea, "Investigation on the effect of geometric parameter on reinforced concrete exterior shear wall-slab connection using finite element analysis," *Advances in Civil Engineering*, vol. 2022, Article ID 4903650, 17 pages, 2022.

[40] S. Dassault, *Abaqus Analysis User's Manual*, Simula Corporation, Oslo, Norway, 2007.